The *SF3B1*^{R625H} Mutation Promotes Prolactinoma Tumor Progression Through Aberrant Splicing Of *DLG1*

Jing Guo
Beijing Neurosurgical Institute
Qiuyue Fang
Beijing Neurosurgical Institute
Yulou Liu
Beijing Neurosurgical Institute
Dawei Wang
Beijing Neurosurgical Institute
Chuzhong Li
Beijing Tiantan Hospital
Weiyan Xie
Beijing Neurosurgical Institute
Yazhuo Zhang (zhangyazhuo@ccmu.edu.cn)
Beijing Neurosurgical Institute

Research Article

Keywords: SF3B1 mutation, Prolactinomas, Alternative splicing, DLG1, Invasion

Posted Date: September 28th, 2021

DOI: https://doi.org/10.21203/rs.3.rs-934219/v1

Version of Record: A version of this preprint was published at Journal of Experimental & Clinical Cancer Research on January 17th, 2022. See the published version at https://doi.org/10.1186/s13046-022-02245-0.

Abstract

Background

Recently, a hotspot mutation in prolactinoma was observed in splicing factor 3b subunit 1 (*SF3B1*^{R625H}), but its functional effects and mechanisms are poorly understood.

Methods

Using the CRISPR/Cas9 genome editing system and rat pituitary GH3 cells, we generated heterozygous *Sf3b1*^{R625H} mutant cells. Sanger and whole-genome sequencing were conducted to verify the introduction of this mutation. Transcriptome analysis was performed in *SF3B1*-wild-type versus mutant human prolactinoma samples and GH3 cells. Quantitative PCR and minigene reporter assays were conducted to verify aberrant splicing. The functional consequences of *SF3B1*^{R625H} were evaluated *in vitro* and *in vivo*. Critical makers of epithelial-mesenchymal transition and key components of relevant signaling pathways were detected by western blot, immunohistochemistry, and immunofluorescence, and were knocked down by siRNA-mediated silencing.

Results

Transcriptomic analysis of prolactinomas and heterozygous mutant cells revealed that the *SF3B1*^{R625H} allele led to different alterations in splicing properties, affecting different genes in different species. Consistently between rat cells and human tumor samples, mutant SF3B1 promoted aberrant splicing and the suppression of DLG1. Additionally, mutant SF3B1 with knockdown of DLG1 expression promoted cell migration, invasion, and epithelial-mesenchymal transition by activating the PI3K/Akt pathway.

Conclusions

Our findings elucidate a mechanism through which mutant *SF3B1* promotes tumor progression and may provide a potent molecular therapeutic target for prolactinomas with the *SF3B1*^{R625H} mutation.

Background

Pituitary adenomas account for between 10% and 20% of intracranial neoplasms, with prolactinomas being the most common subtype[1, 2]. Except for hyperprolactinemia, a subset of prolactinomas are characterized by tumor invasion, resistance to conventional therapy, and high recurrence[3]. Therefore, deciphering the underlying pathogenesis of prolactinoma and determining efficient treatment targets are of great significance to the clinical management of prolactinoma patients.

Alternative splicing is an essential step in the posttranscriptional regulation of gene expression that is a highly regulated and complex process that diversifies the proteome by creating multiple proteins from the same gene[4, 5]. Mutations in splicing factor cause aberrant alternative splicing, which is a key molecular characteristic of tumorigenesis[6]. Splicing factor 3b subunit 1 (SF3B1) is a core component of the U2 small nuclear ribonucleoprotein complex (U2 snRNP), which is essential for pre-mRNA splicing[7]. Recurrent somatic mutations in *SF3B1* have been reported in myelodysplastic syndrome (MDS), chronic lymphocytic leukemia (CLL), and some solid tumors such as uveal melanoma, breast carcinoma, pancreas adenocarcinoma, and others[8–13]. Mutant SF3B1 leads to splicing defects that result in aberrantly spliced transcripts[14]. Approximately half of the aberrantly spliced mRNAs are subject to nonsense-mediated decay (NMD), which causes gene and protein production to be downregulated[15]. Our previous study found a recurrent $SF3B1^{R625H}$ mutation in prolactinoma, which was associated with poor progression-free survival (PFS) and higher levels of prolactin (PRL)[16]. However, the underlying molecular mechanisms of this SF3B1 mutation and its downstream cellular processes in prolactinoma remain unclear.

Herein, we generated a heterozygous $Sf3b1^{R625H}$ mutant rat cell line using CRISPR/Cas9 genome editing technology. RNA sequencing analysis revealed that while *SF3B1* was conserved between rat and human, the aberrantly spliced mRNAs and affected genes differed significantly. Our results suggest that *SF3B1* mutations in prolactinoma stimulate PI3K/AKT signaling by downregulating Discs large 1 (DLG1), which is induced by aberrant splicing and enhances the invasion and migration of tumor cells.

Methods

Cell culture and generation of *Sf3b1* mutant R625H cells

The GH3 rat pituitary cell line was purchased from the American Type Culture Collection (CLL-82.1; Manassas, VA, USA) and was cultured in Ham's F12K medium with 2.5% fetal bovine serum (FBS) and 15% horse bovine serum (Gibco, Waltham, MA, USA). MCF7 and HEK293T cells were obtained from the National Infrastructure of Cell Line Resource (Beijing, China) and were cultured in DMEM (Gibco) supplemented with 10% FBS. PRL levels in cell culture supernatant were detected using an ELISA kit (BioVision, Milpitas, CA, USA) according to the manufacturer's instructions.

The CRISPR/Cas9 gene editing system was used to generate the *Sf3b1* p.R625H (c.G1874A, c.A1875T) mutant GH3 cell line. A Sanger Centre CRISPR webtool (http://www.sanger.ac.uk/htgt/wge/) was used to identify two small guide RNAs (sgRNAs). Cas9/sgRNA-mediated DNA double-strand break and homologous recombination contributed to generated the specific mutation. The 5' sgRNA sequence was 5'-GGCAAGATTCCTTCCTCA-3' and the 3' sgRNA sequence was 5'-GGTTAAGAGTACTGTTGTC-3'. The sgRNA pairs were cloned into a wild-type spCas9 and sgRNA expression plasmid. The donor plasmid (CL-GJ-016-puro-ΔTK) consisted of a puromycin resistance cassette flanked by two *loxP* sites and ~ 1 kb homology arms at both ends of the c. 1874 G > A, c. 1875 A > T mutant exon 14 (Wuhan Genecreate Biological Engineering Co. Ltd., Wuhan, China) (Fig. 1). The plasmid was constructed according to

previously published protocols and confirmed by sequencing. The Neon Transfection System (Thermo Fisher Scientific, Waltham, MA, USA) with pulse voltage of 1000 V for 40 ms was used to co-transfect GH3 cells on a 10-cm plate with 1 μg of CL-GJ-016-puro-TK and 3 μg of Cas9/sgRNA. The cells were screened with puromycin (0.5 μg/mL) starting 48-h post-transfection. Thereafter, single-cell cloning was performed in a 96-well plate. Sanger sequencing was performed using genomic DNA to confirm the specific mutations (DIA-UP Biotech, Beijing, China). Primers were designed to amplify exon 14 of the *Sf3b1* gene (Table S1).

Adenoviral constructs and primary cell culture of human prolactinomas

The adenoviral constructs for mutant *SF3B1*^{R625H} and wild-type *SFB31* were generated by BAC Biological Technology (Beijing, China), and primary cultures of human prolactinoma cells were prepared as described in our previous publication[16]. Tumor cells were infected with adenovirus at a multiplicity of infection of 100, and then harvested for quantitative (q)PCR 48-h later.

RNA sequencing

For GH3 cells, total RNA was extracted using the AllPrep® DNA/RNA Mini kit (QIAGEN, Hilden, Germany) according to the manufacturer's instructions. Sequencing libraries were generated using NEBNext® Ultra™ Directional RNA Library Prep Kit for Illumina® (NEB, Ipswich, MA, USA). The libraries were sequenced on an Illumina platform, and 150-bp paired-end reads were generated. Clean reads were mapped to the Rat Rnor_6.0 genome using Hisat2 (v2.0.5) to obtain read counts, fragments per kilobase per million mapped fragments (FPKM), and transcripts per million (TPM) for each sequenced gene.

Differential alternative splicing and differential gene expression analyses

Differentially expressed genes (DEGs) were identified using DESeq2 using $P < 0.05$ and absolute value of fold change ≥ 1.5. For alterative splicing analysis, rMATS (version 4.0.2)[17] was used to identify alternative splicing events by quantifying exon-exon junction spanning reads on annotated splice junctions present in the rat GENCODE Rnor_6.0 assembly. Differentially spliced mRNAs were defined as FDR < 0.05 and a minimum inclusion level difference > 10% or < − 10%. Three mutant GH3 replicates and three wild-type replicates were compared. Data of two prolactinoma patients with the *SF3B1*^{R625H} mutation and two wild-type cases were selected for alternative splicing analysis, and two mutant and 13 wild-type cases from our previously reports were selected for differential expression analysis[16]. Basic clinic data of these patients are listed in Table S2. Functional enrichment analysis was performed using Gene Ontology (GO) and the Kyoto Encyclopedia of Genes and Genomes (KEGG) to predict the biological functions of DEGs and differentially spliced transcripts. The GO terms analyzed included biological process, cellular components, and molecular functions. A KEGG pathway with a P value < 0.05 was considered to be significant.

Whole-genome sequencing and variant identification

Genomic DNA was extracted from wild-type and mutant GH3 cells using the Blood & Cell Culture DNA Mini Kit (QIAGEN). DNA was sequenced using an Illumina HiSeq 2000, generating 150-bp paired reads. Reads were aligned to the Rat Rnor_6.0 genome using Burrows–Wheeler Aligner (BWA)[18]. SAMtools was used to generate BAM files[19]. Visual inspection of the *Sf3b1* R625H mutation was performed using the Integrative Genomics Viewer[20].

Minigene assay

A DNA fragment containing the *DLG1* exon 22 genomic sequence with 151 bp of flanking intron 21 and 271 bp of flanking intron 22 was inserted between the *KpnI* and *EcoRI* restriction sites of the pcMINI vector to produce the DLG1 minigene construct. Sanger sequencing was performed to confirm the sequence of the inserted fragment. Briefly, the *DLG1* minigene and an adenoviral vector were co-transfected into 293T cells. After 48 h, RNA was harvested for PCR analysis. PCR products were separated by 2% agarose gels and confirmed by Sanger sequencing. The primers used for the spliced products were: 5'-CTAGAGAACCCACTGCTTAC-3' (forward) and 5'-TAGAAGGCACAGTCGAGG-3' (reverse).

Transfection

RIBOBIO (Guangdong, China) synthesized small interfering (si)RNA duplexes; siRNA sequences of rat and human *DLG1* are listed in Table S2. The *Dlg1* overexpressed plasmid, pLV-hef1a-Puro-WPRE-CMV-Dlg1-3×FLAG, was constructed by Beijing Syngentech Co., Ltd. (Beijing, China). All transfections (siRNAs and overexpression plasmids) were performed using Lipofectamine® 3000 Transfection Reagent (Invitrogen, Carlsbad, CA, USA) according to the manufacturer's protocols. Cells were transfected with siRNA or plasmids for 48–72 h. and then collected for qPCR and western blot assays.

Reverse transcription PCR and qPCR

The RNeasy Mini Kit (QIAGEN) was used to extract total RNA and the High Capacity cDNA Reverse Transcription Kit (Thermo Fisher Scientific) was used to generate cDNA, both according to the manufacturers' instructions. For reverse transcription PCR, amplification was performed with I-5 High-Fidelity Master Mix (MCLAB, San Francisco, CA, USA) and specific primers. PCR products were separated on 1–3% agarose gels. All qPCR assays were performed using Power SYBR™ Green PCR Master Mix (Thermo Fisher Scientific) and were analyzed using QuantStudio 3 and 5 systems (Applied Biosystems, Waltham, MA, USA). The comparative Ct method was used to evaluate relative gene expression. The primers used in this study are listed in Table S3.

Scanning electron microscopy (SEM)

SEM was used to examine the external morphological alterations of *Sf3b1* wild-type and mutant GH3 cells. Cells were collected and fixed with 2.5% glutaraldehyde (Solarbio, Beijing, China) at 4°C overnight for SEM preparation. After rinsing with PBS and sterile water, the cells were dehydrated using an ethanol

gradient. The samples were coated with gold after critical point drying, and electron micrographs were taken on a Hitachi SU8020 SEM (Tokyo, Japan).

Cell migration and wound-healing assays

Cell migration culture dish inserts from Ibidi (Martinsried, Germany) were used to conduct wound-healing assays. After 24 h of transfection, cells were seeded into the chambers of the culture dish inserts. The inserts were removed on the next day, and fresh culture medium was added to each well. Scratches were photographed at different points in time using a Zeiss microscope (Oberkochen, Germany).

Sf3b1 mutant and wild-type GH3 cells were seeded onto Imagelock 96-well plates (Essen Bioscience, Ann Arbor, MI, USA). The IncuCyte® Wound Maker (Essen Bioscience) was used to make uniform wounds in a monolayer of confluent cells. Phase contrast imaging was performed every 12 h for a total of 96 h. Images were analyzed using IncuCyte® S3 2018B-2019A software (Essen Bioscience), and data were analyzed using GraphPad Prism7 (GraphPad Software, Inc., La Jolla, CA, USA).

Transwell assays

Transwell plates and Matrigel-coated transwell plates (Corning-Costar, Corning, NY, USA) were used to determine cell migration and invasion capabilities, respectively. Briefly, HEK293T cells resuspended in serum-free medium were inoculate into the upper chamber, and DMEM with 10% FBS was placed in the bottom chamber. Following 24 h of culture, cells on the bottom surface of the chamber were stained with crystal violet and counted under a microscope (Zeiss).

Western blot analysis

Protein samples were separated on 8–10% Bis-Tris SDS-PAGE gels and transferred to polyvinylidene fluoride membranes (Merk, Kenilworth, NJ, USA). All primary antibodies (Table S4) were diluted in TBST containing 1% bovine serum albumin (BSA) and were incubated with the membranes overnight at 4°C. Immunoreactive bands were visualized by chemiluminescence.

Immunohistochemistry

Human prolactinoma tumor specimens were used to examine DLG1, E-cadherin, and Snail protein levels in *SF3B1* wild-type and mutant tumor tissues. The primary antibodies used are summarized in Table S4. Immunohistochemistry was performed by the Leica Bond Polymer Refine Detection system (Leica Biosystems, Wetzlar, Germany). All slides were scanned into digital images, and expression was examined using Aperio AT2 (Leica Biosystems). Staining intensity was scored as 0 (negative), 1 (weak), 2 (moderate), or 3 (strong). The percentage of immunostaining was recorded, and H-scores were calculated using the formula: H-score = 1 × (% weakly stained cells) + 2 × (% moderately stained cells) + 3 × (% strongly stained cells)], ranging from 0 to 300.

Rat prolactinoma model

Rat pituitary tumors were induced by subcutaneously implanting 1-cm silastic capsules containing 10 mg of 17-β estradiol in 4-week-old female F344 rats. Prolactinomas were induced by 17β-estradiol for 5 weeks, as described in our previous report[21]. All experimental protocols were approved by the Animal Use and Care Committee of Beijing Tiantan Hospital. Five weeks later, the prolactinomas were validated via 7.0-T magnetic resonance imaging (MRI) before intra-pituitary injection. The rats were anaesthetized and then 1 μl of adenovirus vector control, wild-type *SFB31*, or *SF3B1*^{R625H} was stereotactically injected into each bilateral tumor. A second MRI examination was performed 2 weeks later, and all rats were sacrificed to collect tumor tissues for further analysis.

Immunofluorescence staining of rat tumor tissues

First, rats were anaesthetized and heart-perfused with 4% formalin. Tumor tissues were then collected and immersed in 10% sucrose for 2 h, and then incubated in 30% sucrose overnight before freezing in OCT compound. Prior to immunofluorescence staining, frozen 5-μm-thick sections were fixed in ice-cold acetone. Tissue slides were blocked with goat serum and incubated with primary antibodies overnight at 4°C (summarized in Table S4). After washing with PBS, the slides were incubated in Alexa Fluor 488 and 594 secondary antibodies (Invitrogen) for 1 h at room temperature; DAPI was used to visualize nuclei.

Phalloidin staining and confocal microscopy

Cells were plated on confocal dishes coated with poly-L-lysine. After incubation at 37°C for 24 hours, the cells were fixed with 4% paraformaldehyde for 30 min, and then stained with 5 μg/mL Alexa Fluor 488-phalloidin (Invitrogen) to reveal filamentous actin (F-actin) in PBS for 40 min at 37°C. DAPI was used to visualize nuclei, and images were captured by confocal laser-scanning microscopy (Zeiss).

Statistical analysis

All statistical analyses were performed using R v3.4.1 (https://www.r-project.org/) and Prism 7 (GraphPad Software, Inc.). All experiments were performed with at least three biological replicates, and all quantitative data represent mean ± standard deviation (SD). Statistical significance was determined by unpaired Student's *t* test (two groups) or one-way ANOVA (multiple groups). $P < 0.05$ was considered statistically significant.

Results

Generation of *Sf3b1* R625H-mutant cells

Our previous study identified the somatic hotspot mutation *SF3B1*^{R625H} in 19.8% of prolactinomas [16]. To investigate the biological role of the *SF3B1*^{R625H} mutation on prolactinoma development and progression as well as similarities and differences between human and rats, we introduced the *Sf3b1*^{R625H} missense mutation into the rat pituitary cell line GH3 using the CRISPR/Cas9 gene editing system (Figure S1A). After isolating and expanding single cell clones, a heterozygous *Sf3b1*-R625H mutation in GH3 cells was confirmed by Sanger sequencing (Fig. 1A). Furthermore, whole-exome

sequencing analyses of the mutant cell line also validated the heterozygous *Sf3b1* mutation, p.R625H (NC_005108.4:g.61608130T > A, g.61608131C > T, NM_053426.1:c.1874G > A, c.1875A > T), and the frequency of the mutant allele obtained from read counts of whole-exome sequencing was 28.57% (18 A&T and 45 G&A, Figure S1B). Additionally, to determine whether heterozygous *Sf3b1*-R625H mutation status affected PRL secretions, we performed ELISA to test PRL levels in culture media from wild-type and mutant cells. Consist with our previously reported results of mutant human prolactinoma[16], PRL levels in supernatant from *Sf3b1* mutant cells was higher compared with wild-type cells (Fig. 1B). Together, these data demonstrate successful construction of a rat cell line model harboring the *Sf3b1*-R625H mutation to model human *SF3B1*-mutant prolactinoma.

Heterozygous *Sf3b1*-R625H status altered the transcriptome of GH3 cells

To explore transcriptome-level alterations in *Sf3b1*-R625H mutant cells, we conducted RNA-seq analysis from wild-type and mutant cultured cells. Using $P < 0.05$ and |fold change|>1.5, we identified 3058 DEGs, with 1271 upregulated and 1787 downregulated genes (Figure S2A; Table S5). Clustering analysis showed distinctly different gene expression patterns between wild-type and *Sf3b1*-mutant cells (Figure S2B). Moreover, compared with *SF3B1*-wild-type patient samples ($n = 13$), we identified 1062 downregulated and 599 upregulated genes in *SF3B1*-mutant human prolactinomas ($n = 2$) with $P < 0.05$ and |fold change|>1.5 (Figure S2C, 2D; Table S6). Comparing the two datasets, we found that only approximately 9% (285/3055) of the DEGs overlapped between rat GH3 cells and human prolactinoma samples (Fig. 1C).

Previous studies have described that the alternative splicing defects caused by cancer-associated *SF3B1* mutations involve incorrect recognition of the 3' splice site, producing aberrant transcripts [15, 22, 23]. To determine whether *Sf3b1*-R625H is associated with mutation-specific alterations in pre-mRNA splicing, we performed percent spliced-in (PSI) analyses of alternative splicing using the rMATS tool[17]. At a False Discovery Rate (FDR) of < 0.05 and |ΔPSI|>0.1, we obtained 143 alternative splicing events in *Sf3b1*-R625H cells (Fig. 1D, Table S7), with exon skipping being the most frequent event (Fig. 1E). GO functional analysis of the alternatively spliced genes revealed enrichment of ontologies including lamellipodium organization, regulation of cell morphogenesis, and motor activity (Fig. 1F, Table S8). We also performed qPCR to confirm several alternative splicing-associated changes (Figure S3A). Additionally, re-analysis of RNA-seq data generated from two *SF3B1*-mutant and two *SF3B1*-wild-type prolactinoma cases[16] uncovered 2287 alternative splicing events in *SF3B1*-mutant cases, with a higher proportion of inclusion alternative 3' splice site (ΔPSI > 10%) and inclusion retained intron (ΔPSI > 10%) events (Fig. 1G; Figure S3B-C; Table S9-10). Similar to human data, *Sf3b1* mutant GH3 cells had more inclusion ($n = 83$, ΔPSI > 10%) than exclusion ($n = 60$, ΔPSI < − 10%) alternative splicing events compared with wild-type cells (Fig. 1E and G). Even so, there was minimal overlap between aberrantly spliced genes, and only approximately 15% (18/120) of the aberrantly spliced genes in rat *Sf3b1*-mutant GH3 cells were common to human samples (Fig. 1H). These data indicate that the limited conservation between rat and human intronic

sequences caused the mutant SF3B1 to have different effects on alternative mRNA splicing in the two species.

The R625H mutation induced epithelial-mesenchymal transition (EMT) phenotypes in tumor cells

Our previous study found that most *SF3B1*-mutant tumors exhibit invasive behavior, which is associated with poor PFS in prolactinoma[24]. Furthermore, GO enrichment analysis of the DEGs and alternative splicing events derived from GH3 cells revealed that cell adhesion molecules and lamellipodium organization were significantly altered in *Sf3b1*-mutant GH3 cells (Figs. 2A and 1F, Tables S8 and S11). These results indicated that *SFB31*-mutant tumor cells have invasive characteristics. To examine changes in the adhesive properties of mutant cells, SEM was performed. Compared with *Sf3b1* wild-type cells, which showed a relatively rounded morphology, *Sf3b1* mutant cells showed prominent lamellipodial extensions (Fig. 2B). Furthermore, F-actin polymerization and filopodium formation were observed in *Sf3b1* mutant cells (Fig. 2B). Lamellipodia formation and dramatic reorganization of the actin cytoskeleton are involved in EMT, which is associated with tumor cell invasion and metastasis[25, 26]. To explore whether *Sf3b1* mutation promotes cell migration, wound-healing assays was conducted. The migration ability of *Sf3b1* mutant cells was significantly enhanced compared with wild-type cells (Fig. 2C). Moreover, the influence of *Sf3b1* mutation on cell migration was also verified by the IncuCyte ZOOM® 96-well Scratch Wound cell migration assay (Fig. 2D).

To determine whether the *Sf3b1* mutation modulated cell migration and invasion through the EMT pathway, we analyzed EMT maker expression. We observed a significant decrease in mesenchymal maker expression and an increase in epithelial maker expression in mutant cells. Immunoblotting of *Sf3b1* mutant cells revealed downregulated expression of E-cadherin along with elevated expression of N-cadherin, Vimentin, and Snail (Fig. 2E). Consistently, immunohistochemistry of consecutive sections from wild-type and mutant prolactinoma tissues supported these findings (Fig. 2F). E-cadherin expression levels yielded an H-score of 146.7 ± 17.64 in wild-type samples and 53.3 ± 14.53 in mutant samples ($P = 0.015$). The H-scores of Snail were 20 ± 5.78 and 196.7 ± 20.28, respectively ($P = 0.0011$). To explore if *SF3B1*-R625H promoted EMT of prolactinoma *in vivo*, F344 rat prolactinomas were induced by 6-weel 17β-estradiol treatment. Then the rat prolactinomas were stereotactically injected with wild-type and R625H *SF3B1* encoding adenoviruses and negative controls. After 2 weeks, tumors were collected and immunofluorescence was used to examine EMT maker expression. Decreased levels of E-cadherin and increased levels of Vimentin were observed in the R625H groups (Fig. 2G). Overall, these data demonstrated that mutant SF3B1 promoted EMT.

To explore the molecular mechanisms through which the *SF3B1* mutation induced EMT, we analyzed the intersection of aberrantly spliced genes and DEGs in rat GH3 cells and human prolactinoma samples (Fig. 2H). From this intersection, *DLG1* was the only identified gene (Fig. 2H), and was significantly downregulated and mis-spliced in *SF3B1* mutants (Tables S5–S7 and S9).

Mutant SF3B1 caused aberrant splicing of *DLG1*

DLG1 is a member of the molecular scaffold protein family knows as membrane associated guanylate kinases (MAGUKs)[27]. DLG1 is a component of the conserved Scribble polarity complex, which is associated with the establishment and maintenance of cell polarity and is defined as a potential tumor suppressor[28, 29]. To confirm that aberrant splicing of *DLG1* was caused by *SF3B1* mutation, RNA-seq data from human prolactinoma and GH3 cells was examined. Across human prolactinoma, aberrant splicing of *DLG1* was induced by mutant SF3B1 through usage of a cryptic 3' splice site (Fig. 3A; Table S9), which was confirmed by qPCR in prolactinoma patient samples (Fig. 3B). To verify the effect of mutant SF3B1 on *DLG1* in vitro, we infected primary cultured pituitary tumor cells with adenovirus carrying the *SF3B1*-R625H mutation, and the results showed that the cryptic *DLG1* transcript was observed in the Ad-SF3B1-R625H group (Fig. 3C). The same results were also observed in HEK293T cells (Fig. 3D and S4A). To verify differences between the wild-type and mutant alleles, we performed TA cloning. Through reverse transcription PCR and sequencing clones, we confirmed that the Ad-SF3B1-R625H group included more abnormal PCR products than the Ad-SF3B1-WT group (Figure S4B). The expected fragment with a 16-bp extension of exon 22 was identified by Sanger sequencing of PCR products (Fig. 3E). We then generated a minigene construct that contained sequences from the misspliced intron and flanking exon to explore alternative splicing (Fig. 3F). After co-transfection into HEK293T cells, a complete spliced RNA containing exon 22 was observed in the *SF3B1*-WT and control groups (Fig. 3G, left and middle lanes); however, a larger transcript was observed in the *SF3B1*-R625H group that retained an extra 16 bp (Fig. 3G, right lane). The extra 16-bp fragment was confirmed by Sanger sequencing (Fig. 3H). Additionally, mutually exclusive splicing of *Dlg1* in *Sf3b1*-mutant GH3 cells was confirmed by reverse transcription PCR (Fig. 3I; Table S7). These data identified that mutant *SF3B1* induced aberrant splicing of *DLG1*.

To verify whether the *SF3B1* mutation altered *DLG1* expression, RNA-seq data was examined and qPCR was performed in *SF3B1* mutant samples. These data revealed that *DLG1* was downregulated in *SF3B1*-mutant human prolactinoma samples and GH3 cells (Fig. 4A, B). Furthermore, immunohistochemistry and western blotting revealed that DLG1 protein expression was decreased in *SF3B1*-mutant human samples and GH3 cells (Fig. 4C and 2E). The H-scores of DLG1 were 153 ± 17.64 in human *SF3B1*-wild-type and 40 ± 20.82 in human *SF3B1*-mutant samples (P = 0.0142). To further confirm the effect of the *SF3B1* mutation on DLG1 expression, immunofluorescence was performed on tumors stereotactically injected with adenoviruses. Decreased DLG1 expression was observed in the Ad-SF3B1 R625H group (Fig. 4D). Taken together, these data demonstrate that mutant SF3B1 induced aberrant splicing and reduced expression of *DLG1*.

Knocking down *DLG1* promoted cell migration, invasion, and EMT

To evaluate the role of DLG1 in tumor cell invasion and migration, we knocked down *DLG1* by transfecting specific siRNAs. Both the mRNA and protein levels of DLG1 were efficiently depleted in GH3, 293T, and MCF7 cells (Fig. 5A-B). Western blot results revealed that knocking down *DLG1* promoted EMT by decreasing the expression of E-cadherin and increasing the expression of N-cadherin, Vimentin, and Snail (Fig. 5B). Furthermore, restoring DLG1 expression in wild-type and mutant GH3 cells inhibited the EMT program (Fig. 2E). Wound healing assays revealed that si-DLG1-transfected cells traversed wounds significantly faster than the si-NC-transfected cells (Fig. 5C). Comparable migration differences were also observed in the transwell assay (Fig. 5D). In transwell Matrigel invasion assays, significantly more si-DLG1-transfected cells migrated through the Matrigel layer (Fig. 5D). Furthermore, phalloidin staining showed differences in F-actin organization at the wound margin. Compared with si-NC-transfected cells, si-DLG1-transfected cells showed polarized lamellipodia formation *via* F-actin (phalloidin) staining (Fig. 5E). These results suggested that depleting DLG1 enhanced tumor cell migration and invasion, and induced EMT.

The SFB31/DLG1 axis promoted tumor invasion *via* the PI3K/AKT pathway

To determine the key biological mechanism through which mutant SF3B1 promoted prolactinoma progression, we performed a function enrichment analysis of the DEGs from human tumors and rat GH3 cells. This revealed that PI3K/AKT signaling was significantly altered in mutant SF3B1 samples compared with wild type samples (Fig. 6A, Tables S12-13). We therefore detected the relevant effectors within this pathway through western blotting and found increased phosphorylation of AKT (T308) and GSK-3β in *Sf3b1*-mutant GH3 cells (Fig. 6B). To clarify the specific role of DLG1 in activation of the PI3K/AKT pathway in tumor cells, we manipulated DLG1 activity in GH3, 293T, and MCF7 cells. Knocking down *DLG1* in cells by siRNA increased phosphorylation of AKT and GSK-3β (Fig. 6C). Furthermore, restoration of DLG1 expression in wild-type and mutant GH3 cells showed reduced phosphorylation of AKT and GSK-3β (Fig. 6B). Thus, these data strongly suggest that altering DLG1 levels due to alternative splicing induced by mutant SF3B1 promotes PI3K/AKT signaling in prolactinoma.

Discussion

SF3B1 is the most frequently mutated splicing gene in cancer, with three major hotspots: the codon positions K700, R625, and R622[30]. Among these mutated codons, K700E is the most common mutation in CLL, MDS, acute myeloid leukemia, and invasive breast carcinoma, while R625 is the predominant mutation in uveal melanoma and skin cutaneous melanoma[31]. Previous studies have explored how the $SF3B1^{K700E}$ mutation contributes to aberrant splicing and downstream pro-tumorigenesis mechanisms in CLL and breast cancer using cell lines and mouse disease models[31, 32]. To understand the molecular and phenotypic consequences of the $SF3B1^{R625H}$ mutation on prolactinoma tumorigenesis, we generated

a heterozygous *Sf3b1*-R625H mutant rat pituitary cell line. We then demonstrated that heterozygosity for *Sf3b1*-R625H in GH3 cells was sufficient to cause characteristic features similar to human prolactinoma, including higher PRL levels and invasive behaviors. Although phylogenetic analysis revealed that the $SF3B1^{R625H}$ locus is highly conserved across species[16], only a few events were shared between mutant human prolactinoma and rat cells. These results may be due to the frequency of the mutant allele in heterozygous mutant cells and relatively poor interspecies conservation of intronic sequences between rats and humans. Moreover, our study found that the majority of aberrant splicing events in *SF3B1* mutant human prolactinoma were retained intron followed by alternative 3' splice site. This is different from previous observations in *SF3B1*-mutant cancers[15, 33], which suggested a higher proportion of alternative 3' splice site events, but were similar to a recent report in *SF3B1*-mutant MDS[14]. Considering the limited number *SF3B1*-mutant human prolactinoma tumor samples, further studies with larger cohorts are needed to confirm these results. In particular, we consistently found that the *DLG1* transcript was shared between rat cells and human prolactinoma samples, with mRNA downregulation and differential missplicing. Interestingly, mutant *SF3B1* induced the inclusion of 16 intronic nucleotides in exon 22 by using an upstream cryptic 3' splice site in human sequences (Fig. 3A), which may lead to NMD and reduced DLG1 expression, because the shifted reading frame produces a premature termination codon in this alternative spliceform[32]. Despite mutant SF3B1 inducing different splicing events in rats and humans, *DLG1* mRNA and protein were downregulated in both models.

Our data demonstrated that downregulating *DLG1* expression promote tumor cell migration and invasion. As previously reported, DLG1 was involved in mammalian tumorigenesis and was localized to adherens junctions in epithelial cells[34]. In mammals, *DLG1* appears to act as a tumor suppressor by affecting other polarity complexes, Myosin II activity, the actin cytoskeleton, and/or other signaling pathways[35–37]. Our studies further indicated that knocking down *DLG1* induced EMT in tumor cells. EMT is well known to be related to the loss of cell polarity, specifically the loss of adherens junctions and enables the development of an invasive phenotype[38]. Consist with our results, the study by Sugihara, T. *et al.* found that loss of DLG1 was associated with poor prognosis in endometrial cancer and that knocking down *DLG1* accelerated tumor migration and invasion *in vitro*[29].

Previous studies have revealed that the AKT/GSK-3β/Snail axis is critical for the induction and maintenance of EMT [39, 40]. In this study, we show that mutant SF3B1 and decreased DLG1 expression activate the PI3K/AKT pathway, which results in tumor cells undergoing EMT and gaining migration and invasive properties (Fig. 7). It is known that p-AKT can suppress GSK-3β activity (through phosphorylation of Ser 9) and stabilize Snail[41]. Furthermore, DLG1 has been demonstrated to modulate the PI3K/Akt pathway to precisely regulate regulatory T cell activity[42]. Consistent with this, we found that low DLG1 expression increased p-AKT, p-G3K-3β, and Snail expression levels, which could be rescued by overexpressing DLG1. Future work comprehensively defining the how DLG1 activates the PI3K/Akt signaling pathway in tumor cell may therefore be very important.

Conclusions

In summary, we confirmed the molecular mechanism through which the *SF3B1*-R625H mutation actives the PI3K/Akt pathway in prolactinoma by aberrant splicing of *DLG1*, which promotes tumor invasion progression. Our findings provide the rationale for investigating new therapeutic strategies in patients with *SF3B1*-mutant prolactinoma.

Abbreviations

MDS Myelodysplastic syndrome

CLL Chronic lymphocytic leukemia

NMD Nonsense-mediated decay

PFS Progression-free survival

FBS Fetal bovine serum

FPKM Fragments per kilobase per million mapped fragments

TPM Transcripts per million

DEGs Differentially expressed genes

GO Gene Ontology

KEGG Kyoto Encyclopedia of Genes and Genomes

BSA Bovine serum albumin

MRI Magnetic resonance imaging

MAGUKs Membrane associated guanylate kinases

Declarations

Ethics approval and consent to participate

The present study was approved by The Ethics Committees of Beijing Tiantan Hospital. All subjects provided written informed consent. The animal experiments were approved by the Animal Use and Care Committee of Beijing Tiantan Hospital.

Consent for publication

Not applicable.

Availability of data and materials

The datasets used and/or analysed during the current study are available from the corresponding author on reasonable request.

Competing interests

The authors declare that they have no competing interests.

Funding

This study was supported by the National Natural Science Foundation of China (Grant codes: 81672495, 81771489, 82072804, 82071559, and 82071558).

Authors' contributions

WX and YZ worked on the conception and designed the research. CL and DW were involved in the collection and analysis of patients' clinical data. JG, QF and YL performed the experiments. JG was dedicated to data analysis, interpretation, and drafting. All authors read and approved the final manuscript.

Acknowledgements

Not applicable.

References

1. Asa SL, Ezzat S: **The cytogenesis and pathogenesis of pituitary adenomas**. *Endocr Rev* 1998, **19**(6):798-827.
2. Daly AF, Rixhon M, Adam C, Dempegioti A, Tichomirowa MA, Beckers A: **High prevalence of pituitary adenomas: a cross-sectional study in the province of Liege, Belgium**. *J Clin Endocrinol Metab* 2006, **91**(12):4769-4775.
3. Vroonen L, Daly AF, Beckers A: **Epidemiology and Management Challenges in Prolactinomas**. *Neuroendocrinology* 2019, **109**(1):20-27.
4. Nilsen TW, Graveley BR: **Expansion of the eukaryotic proteome by alternative splicing**. *Nature* 2010, **463**(7280):457-463.
5. Lee Y, Rio DC: **Mechanisms and Regulation of Alternative Pre-mRNA Splicing**. *Annu Rev Biochem* 2015, **84**:291-323.
6. Sveen A, Kilpinen S, Ruusulehto A, Lothe RA, Skotheim RI: **Aberrant RNA splicing in cancer; expression changes and driver mutations of splicing factor genes**. *Oncogene* 2016, **35**(19):2413-2427.
7. Kramer A: **The structure and function of proteins involved in mammalian pre-mRNA splicing**. *Annu Rev Biochem* 1996, **65**:367-409.

8. Papaemmanuil E, Cazzola M, Boultwood J, Malcovati L, Vyas P, Bowen D, Pellagatti A, Wainscoat JS, Hellstrom-Lindberg E, Gambacorti-Passerini C *et al*: **Somatic SF3B1 mutation in myelodysplasia with ring sideroblasts**. *N Engl J Med* 2011, **365**(15):1384-1395.
9. Wang L, Lawrence MS, Wan Y, Stojanov P, Sougnez C, Stevenson K, Werner L, Sivachenko A, DeLuca DS, Zhang L *et al*: **SF3B1 and other novel cancer genes in chronic lymphocytic leukemia**. *N Engl J Med* 2011, **365**(26):2497-2506.
10. Banerji S, Cibulskis K, Rangel-Escareno C, Brown KK, Carter SL, Frederick AM, Lawrence MS, Sivachenko AY, Sougnez C, Zou L *et al*: **Sequence analysis of mutations and translocations across breast cancer subtypes**. *Nature* 2012, **486**(7403):405-409.
11. Biankin AV, Waddell N, Kassahn KS, Gingras MC, Muthuswamy LB, Johns AL, Miller DK, Wilson PJ, Patch AM, Wu J *et al*: **Pancreatic cancer genomes reveal aberrations in axon guidance pathway genes**. *Nature* 2012, **491**(7424):399-405.
12. Furney SJ, Pedersen M, Gentien D, Dumont AG, Rapinat A, Desjardins L, Turajlic S, Piperno-Neumann S, de la Grange P, Roman-Roman S *et al*: **SF3B1 mutations are associated with alternative splicing in uveal melanoma**. *Cancer Discov* 2013, **3**(10):1122-1129.
13. Armenia J, Wankowicz SAM, Liu D, Gao J, Kundra R, Reznik E, Chatila WK, Chakravarty D, Han GC, Coleman I *et al*: **The long tail of oncogenic drivers in prostate cancer**. *Nat Genet* 2018, **50**(5):645-651.
14. Pellagatti A, Armstrong RN, Steeples V, Sharma E, Repapi E, Singh S, Sanchi A, Radujkovic A, Horn P, Dolatshad H *et al*: **Impact of spliceosome mutations on RNA splicing in myelodysplasia: dysregulated genes/pathways and clinical associations**. *Blood* 2018, **132**(12):1225-1240.
15. Darman RB, Seiler M, Agrawal AA, Lim KH, Peng S, Aird D, Bailey SL, Bhavsar EB, Chan B, Colla S *et al*: **Cancer-Associated SF3B1 Hotspot Mutations Induce Cryptic 3' Splice Site Selection through Use of a Different Branch Point**. *Cell reports* 2015, **13**(5):1033-1045.
16. Li C, Xie W, Rosenblum JS, Zhou J, Guo J, Miao Y, Shen Y, Wang H, Gong L, Li M *et al*: **Somatic SF3B1 hotspot mutation in prolactinomas**. *Nat Commun* 2020, **11**(1):2506.
17. Shen S, Park JW, Lu ZX, Lin L, Henry MD, Wu YN, Zhou Q, Xing Y: **rMATS: robust and flexible detection of differential alternative splicing from replicate RNA-Seq data**. *Proc Natl Acad Sci U S A* 2014, **111**(51):E5593-5601.
18. Li H, Durbin R: **Fast and accurate short read alignment with Burrows-Wheeler transform**. *Bioinformatics* 2009, **25**(14):1754-1760.
19. Li H, Handsaker B, Wysoker A, Fennell T, Ruan J, Homer N, Marth G, Abecasis G, Durbin R, Genome Project Data Processing S: **The Sequence Alignment/Map format and SAMtools**. *Bioinformatics* 2009, **25**(16):2078-2079.
20. Robinson JT, Thorvaldsdottir H, Winckler W, Guttman M, Lander ES, Getz G, Mesirov JP: **Integrative genomics viewer**. *Nat Biotechnol* 2011, **29**(1):24-26.
21. Lei C, Jing G, Jichao W, Xiaohui L, Fang Q, Hua G, Yazhou M, Zhang Y: **MiR-137's Tumor Suppression on Prolactinomas by Targeting MITF and Modulating Wnt Signaling Pathway**. *J Clin Endocrinol Metab* 2019, **104**(12):6391-6402.

22. Wang L, Brooks AN, Fan J, Wan Y, Gambe R, Li S, Hergert S, Yin S, Freeman SS, Levin JZ *et al*: **Transcriptomic Characterization of SF3B1 Mutation Reveals Its Pleiotropic Effects in Chronic Lymphocytic Leukemia**. *Cancer cell* 2016, **30**(5):750-763.
23. Shiozawa Y, Malcovati L, Galli A, Sato-Otsubo A, Kataoka K, Sato Y, Watatani Y, Suzuki H, Yoshizato T, Yoshida K *et al*: **Aberrant splicing and defective mRNA production induced by somatic spliceosome mutations in myelodysplasia**. *Nat Commun* 2018, **9**(1):3649.
24. Kim K, Park YW, Kim D, Ahn SS, Moon JH, Kim EH, Lee EJ, Ku CR: **Biochemical Remission after Cabergoline Withdrawal in Hyperprolactinemic Patients with Visible Remnant Pituitary Adenoma**. *J Clin Endocrinol Metab* 2021, **106**(2):e615-e624.
25. Yilmaz M, Christofori G: **EMT, the cytoskeleton, and cancer cell invasion**. *Cancer Metastasis Rev* 2009, **28**(1-2):15-33.
26. Aiello NM, Maddipati R, Norgard RJ, Balli D, Li J, Yuan S, Yamazoe T, Black T, Sahmoud A, Furth EE *et al*: **EMT Subtype Influences Epithelial Plasticity and Mode of Cell Migration**. *Dev Cell* 2018, **45**(6):681-695 e684.
27. Ivanova S, Gregorc U, Vidergar N, Javier R, Bredt DS, Vandenabeele P, Pardo J, Simon MM, Turk V, Banks L *et al*: **MAGUKs, scaffolding proteins at cell junctions, are substrates of different proteases during apoptosis**. *Cell Death Dis* 2011, **2**:e116.
28. Facciuto F, Cavatorta AL, Valdano MB, Marziali F, Gardiol D: **Differential expression of PDZ domain-containing proteins in human diseases - challenging topics and novel issues**. *FEBS J* 2012, **279**(19):3538-3548.
29. Sugihara T, Nakagawa S, Sasajima Y, Ichinose T, Hiraike H, Kondo F, Uozaki H, Fukusato T, Ayabe T: **Loss of the cell polarity determinant human Discs-large is a novel molecular marker of nodal involvement and poor prognosis in endometrial cancer**. *Br J Cancer* 2016, **114**(9):1012-1018.
30. Alsafadi S, Houy A, Battistella A, Popova T, Wassef M, Henry E, Tirode F, Constantinou A, Piperno-Neumann S, Roman-Roman S *et al*: **Cancer-associated SF3B1 mutations affect alternative splicing by promoting alternative branchpoint usage**. *Nat Commun* 2016, **7**:10615.
31. Liu Z, Yoshimi A, Wang J, Cho H, Chun-Wei Lee S, Ki M, Bitner L, Chu T, Shah H, Liu B *et al*: **Mutations in the RNA Splicing Factor SF3B1 Promote Tumorigenesis through MYC Stabilization**. *Cancer Discov* 2020, **10**(6):806-821.
32. Liu B, Liu Z, Chen S, Ki M, Erickson C, Reis-Filho JS, Durham BH, Chang Q, de Stanchina E, Sun Y *et al*: **Mutant SF3B1 promotes AKT- and NF-kappaB-driven mammary tumorigenesis**. *J Clin Invest* 2021, **131**(1).
33. DeBoever C, Ghia EM, Shepard PJ, Rassenti L, Barrett CL, Jepsen K, Jamieson CH, Carson D, Kipps TJ, Frazer KA: **Transcriptome sequencing reveals potential mechanism of cryptic 3' splice site selection in SF3B1-mutated cancers**. *PLoS Comput Biol* 2015, **11**(3):e1004105.
34. Humbert PO, Grzeschik NA, Brumby AM, Galea R, Elsum I, Richardson HE: **Control of tumourigenesis by the Scribble/Dlg/Lgl polarity module**. *Oncogene* 2008, **27**(55):6888-6907.

35. Peng CY, Manning L, Albertson R, Doe CQ: **The tumour-suppressor genes lgl and dlg regulate basal protein targeting in Drosophila neuroblasts**. *Nature* 2000, **408**(6812):596-600.
36. Bilder D, Schober M, Perrimon N: **Integrated activity of PDZ protein complexes regulates epithelial polarity**. *Nat Cell Biol* 2003, **5**(1):53-58.
37. Hawkins ED, Russell SM: **Upsides and downsides to polarity and asymmetric cell division in leukemia**. *Oncogene* 2008, **27**(55):7003-7017.
38. Lamouille S, Xu J, Derynck R: **Molecular mechanisms of epithelial-mesenchymal transition**. *Nat Rev Mol Cell Biol* 2014, **15**(3):178-196.
39. Lan Y, Han J, Wang Y, Wang J, Yang G, Li K, Song R, Zheng T, Liang Y, Pan S *et al*: **STK17B promotes carcinogenesis and metastasis via AKT/GSK-3beta/Snail signaling in hepatocellular carcinoma**. *Cell Death Dis* 2018, **9**(2):236.
40. Stegeman H, Span PN, Kaanders JH, Bussink J: **Improving chemoradiation efficacy by PI3-K/AKT inhibition**. *Cancer Treat Rev* 2014, **40**(10):1182-1191.
41. Zhou BP, Deng J, Xia W, Xu J, Li YM, Gunduz M, Hung MC: **Dual regulation of Snail by GSK-3beta-mediated phosphorylation in control of epithelial-mesenchymal transition**. *Nat Cell Biol* 2004, **6**(10):931-940.
42. Zanin-Zhorov A, Lin J, Scher J, Kumari S, Blair D, Hippen KL, Blazar BR, Abramson SB, Lafaille JJ, Dustin ML: **Scaffold protein Disc large homolog 1 is required for T-cell receptor-induced activation of regulatory T-cell function**. *Proc Natl Acad Sci U S A* 2012, **109**(5):1625-1630.

Figures

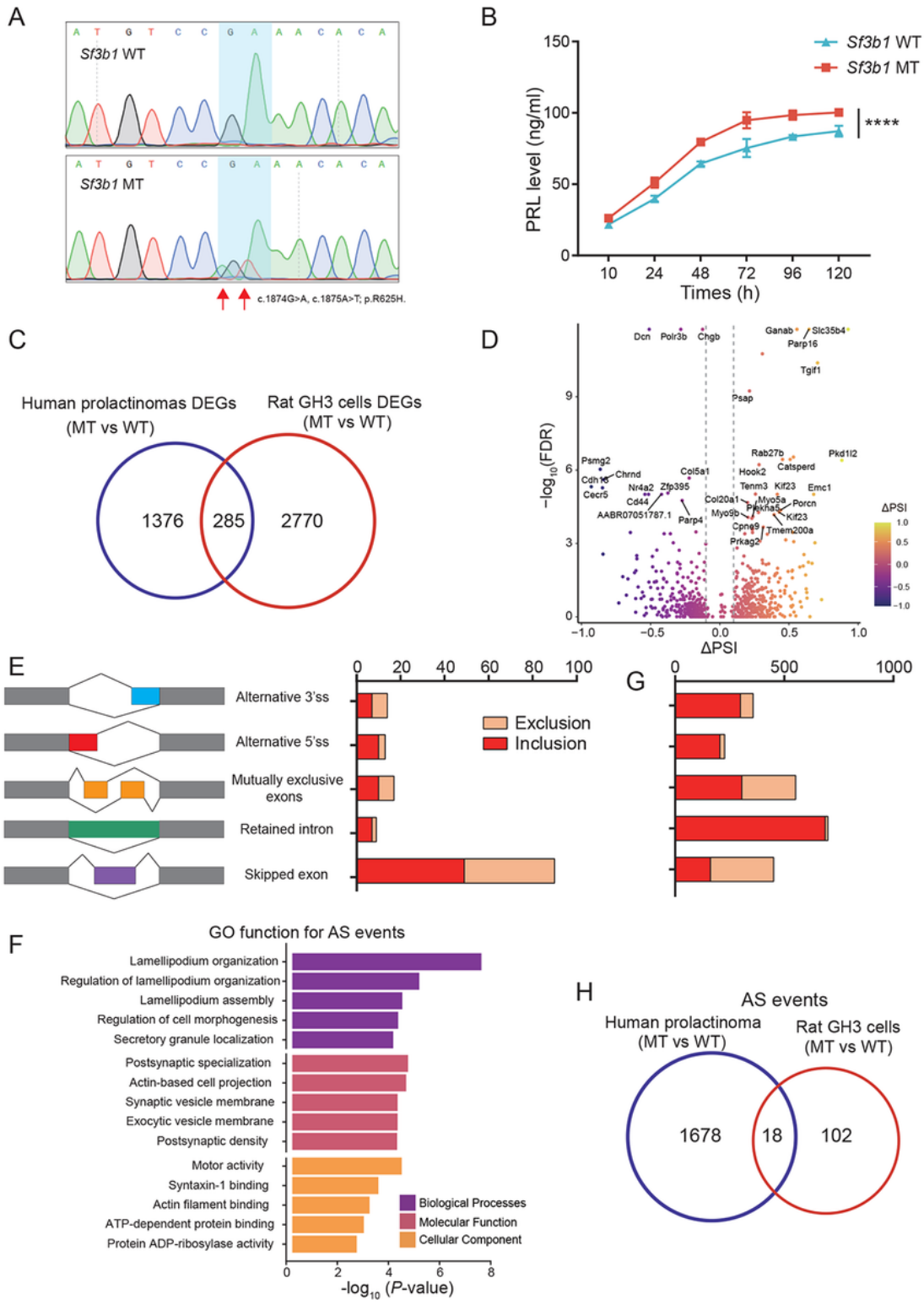

Figure 1

Generation of heterozygous Sf3b1-R625H mutant GH3 cells. (A) Sequencing chromatogram demonstrating the heterozygous Sf3b1-R625H mutation. The homozygous nucleotide in Sf3b1 wild-type GH3 cells and heterozygous nucleotides in Sf3b1 mutant GH3 cells are shown. (B) PRL secretion in Sf3b1 wild-type and mutant GH3 cells are shown. Data are represented as mean ± SD. (P-values by two-way ANOVA, ****P<0.0001). (C) Venn diagram showing the overlapping DEGs identified in SF3B1 mutant

human prolactinoma and GH3 cells. (D) Volcano plot showing the differential alternative splicing events in Sf3b1 mutant vs. wild-type GH3 cells. Significant alternative splicing events identified at FDR <0.05 and |ΔPSI| >0.1. PSI: Percent Splice In. Top 30 significant mis-spliced genes are indicated. (E) Number and type of mis-splicing events in Sf3b1 mutant vs. wild-type GH3 cells are shown. Inclusion: events with ΔPSI>10%; exclusion: events with ΔPSI<−10% (F) GO analysis of mis-spliced genes in Sf3b1 mutant vs. wild-type GH3 cells; the top five ranked terms are shown. (G) Number and type of mis-splicing events in SF3B1 mutant vs. wild-type human prolactinoma. (H) Venn diagram showing the overlap of mis-spliced genes identified in SF3B1 mutant human prolactinoma and GH3 cells.

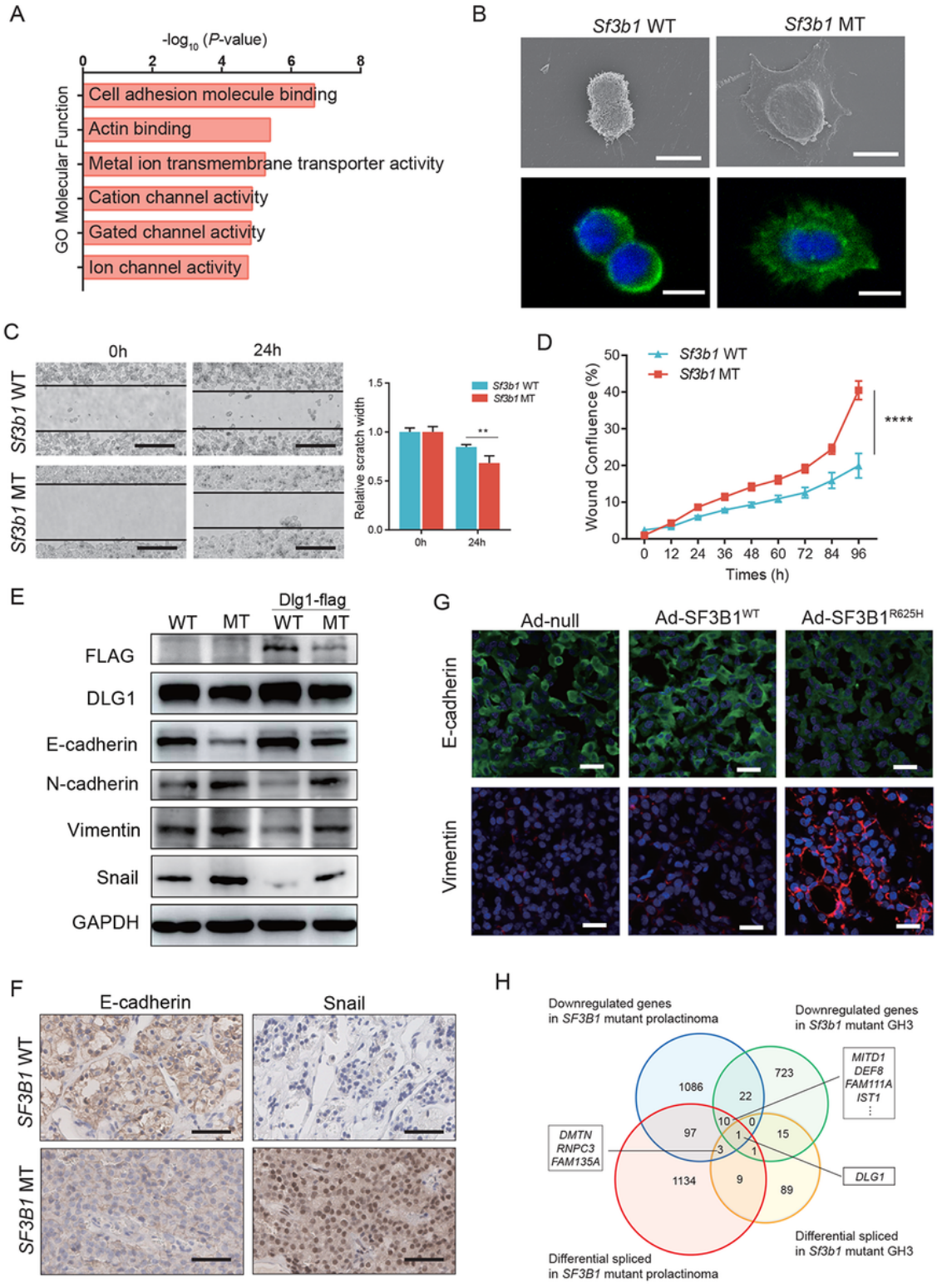

Figure 2

Mutant SF3B1 promoted EMT phenotypes in prolactinoma. (A) GO functional enrichment analysis of DEGs in Sf3b1 mutant vs. wild-type GH3 cells. (B) Scanning electron microscopy (SEM; upper) and confocal images of the actin cytoskeleton stained with rhodamine–phalloidin (lower) of Sf3b1 wild-type and mutant GH3 cells; scale bar: 10 μm. (C) Scratch wound healing assays were performed using Sf3b1 wild-type and mutant GH3 cells; scale bar: 200 μm. Relative scratch widths are shown over time (n=3;

mean ± SD shown below; P values by Student's test). (D) Kinetics of wound confluence over 96 h were analyzed using IncuCyte 2018B software (Essen Bioscience). The results are expressed as mean ± SD, n=3. P values by two-way ANOVA; ****P<0.0001. (E) DLG1, E-cadherin, N-cadherin, Vimentin, and Snail levels in Sf3b1 wild-type and mutant GH3 cells transduced with or without Dlg1-FLAG cDNA. (G) Immunofluorescence staining of E-cadherin and Vimentin in rat prolactinoma tumors stereotactically injected with Ad-null, Ad-SF3B1WT, and Ad-SF3B1R625H; scale bar: 50 μm. (F) Representative immunohistochemical staining for E-cadherin and Snail in SF3B1 mutant and wild-type human prolactinoma tumors; scale bar: 50 μm. (H) Venn diagram of the numbers of differentially spliced (q<0.05; t test) and differentially expressed genes (q<0.05; DESeq2) in SF3B1 mutant human prolactinoma and GH3 samples.

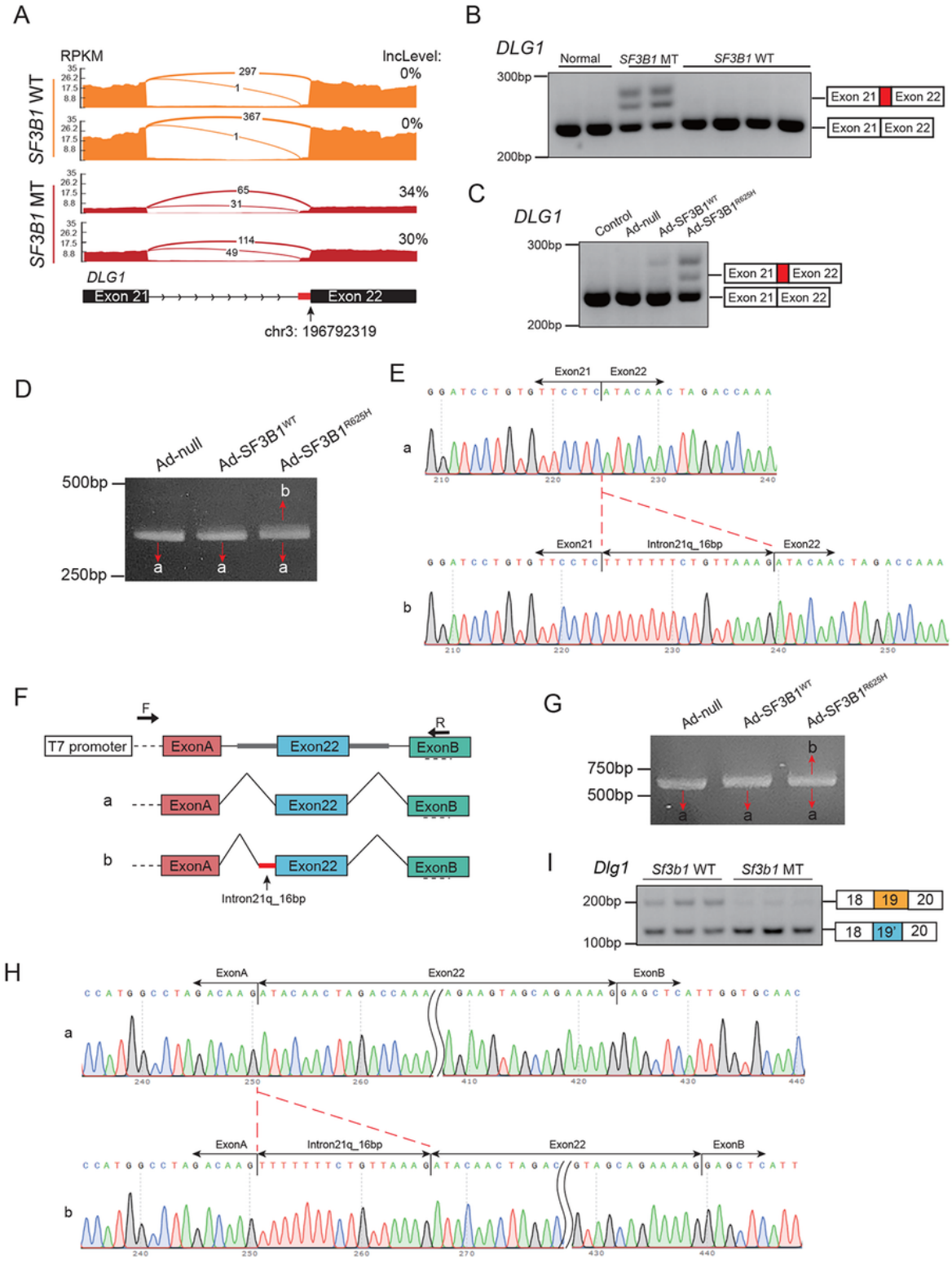

Figure 3

Mutant SF3B1 caused aberrant splicing of DLG1. (A) Sashimi plots of alternative 3' splice sites of DLG1 in representative human prolactinoma with or without SF3B1 mutations. (B) Reverse transcription PCR of DLG1 splicing events in human prolactinoma samples with or without SF3B1 mutation. The 3' splice sites used are shown in the schematic. (C) Reverse transcription PCR results of aberrant DLG1 splicing in primary human prolactinoma cells infected with adenovirus carrying SF3B1-WT and SF3B1-R625H

vectors. (D) Reverse transcription PCR of DLG1 splicing in 293T cells infected with adenovirus carrying SF3B1-WT and SF3B1-R625H vectors. Band a: canonical DLG1 transcript; Band b: aberrant DLG1 transcript. (E) The sequences of gel-purified fragments showing the canonical DLG1 transcript (a) and aberrant transcript (b). (F) Schematic diagram of the minigene construct and schematic diagram of Sanger sequencing of reverse transcription PCR products. (G) Reverse transcription PCR results of DLG1 splicing in 293T cells co-transduced with the minigene reporter and adenovirus carrying SF3B1-WT and SF3B1-R625H vectors. (H) The sequence of gel-purified fragments. The canonical DLG1 transcript (a) and aberrant DLG1 transcript (b) were observed in the SF3B1-WT and SF3B1-R625 groups, respectively. (I) Reverse transcription PCR results of Dlg1 splicing in Sf3b1 mutant GH3 cells. The mutually exclusive splicing type is shown in the schematic.

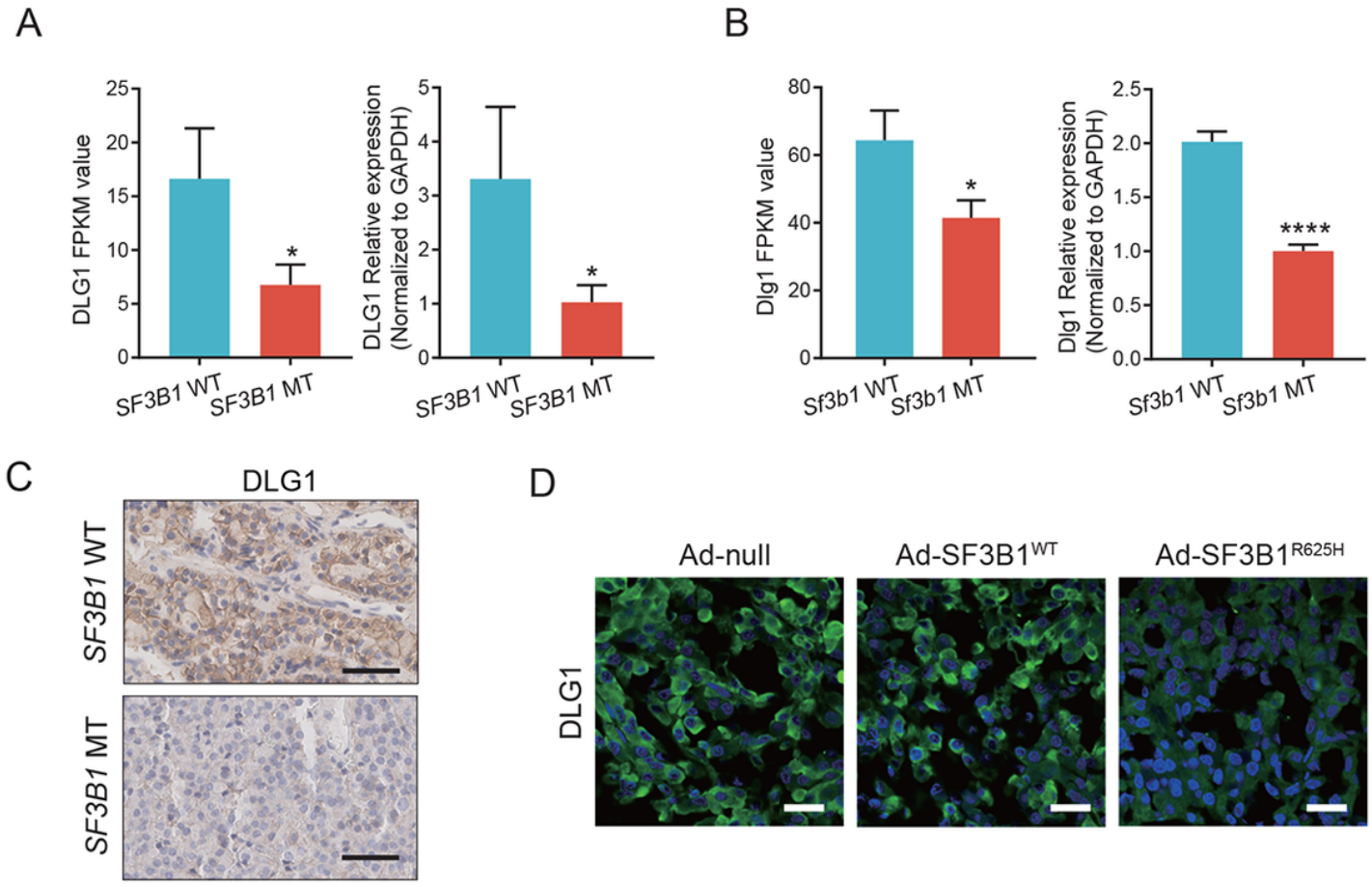

Figure 4

Mutant SF3B1 altered DLG1 expression. (A) DLG1 mRNA expression (RNA-seq data and quantitative PCR) in SF3B1 mutant (n=2) vs. wild-type (n=13) human prolactinoma tumors. (B) DLG1 mRNA expression in Sf3b1 mutant (n=3) versus wild-type (n=3) GH3 cells. TPM: Transcripts per million kilobase. The results are expressed as mean ± SD (Student's t test, *P<0.05, ****P<0.0001). (C) Representative immunohistochemical staining for DLG1 in SF3B1 mutant and wild-type human prolactinoma tumors; scale bar: 50 μm. (D) Immunofluorescence staining for DLG1 in rat prolactinoma tumors stereotactically injected with Ad-null, Ad-SF3B1WT, and Ad-SF3B1R625H, respectively; scale bar: 50 μm.

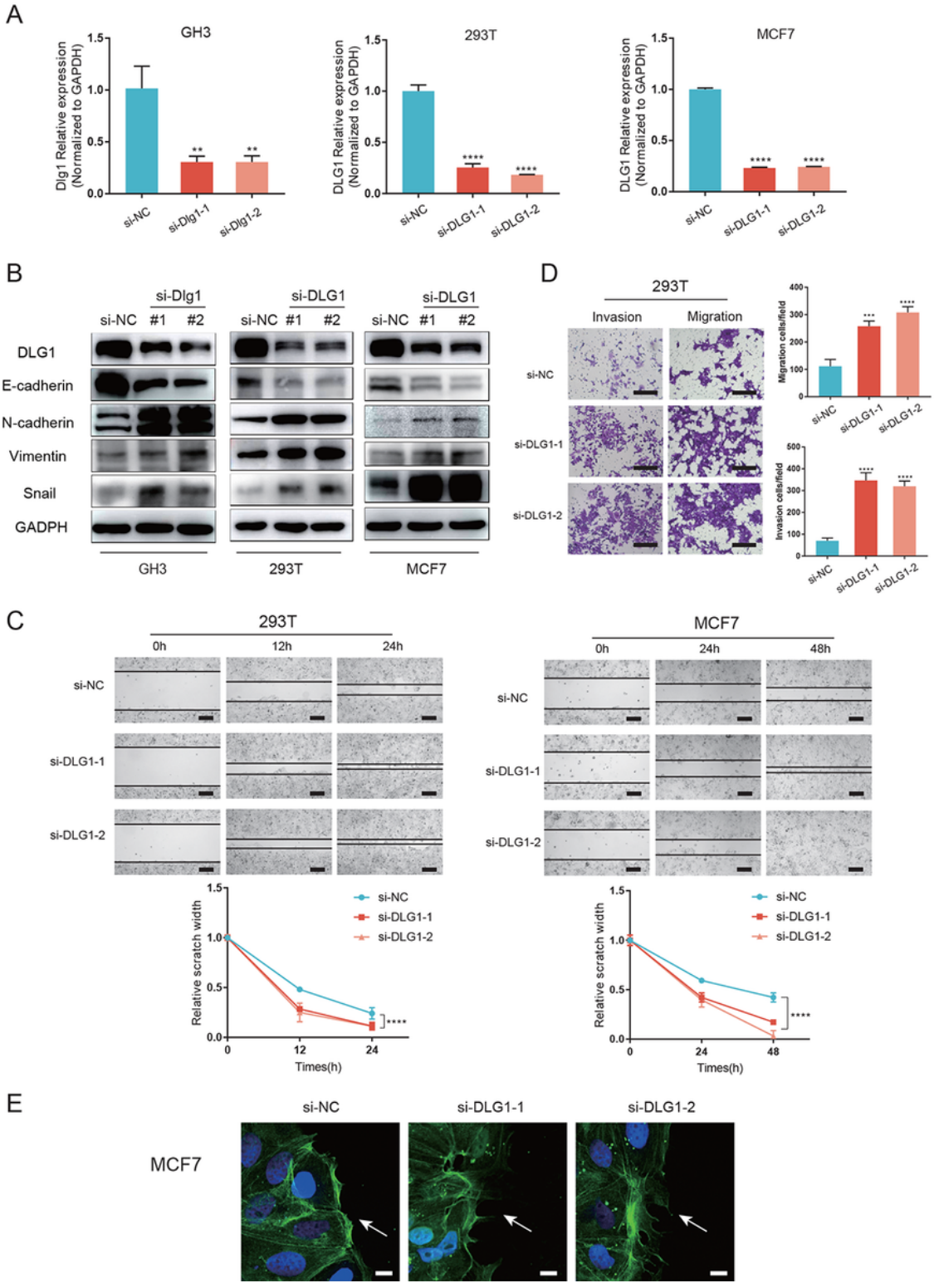

Figure 5

Knocking down DLG1 promoted cell migration, invasion, and EMT. (A) Quantitative PCR analysis of DLG1 knockdown efficiency in GH3, MCF-7, and 293T cells. Results are expressed as mean ± SD; P values by one-way ANOVA compared with control (si-NC). (B) DLG1 knockdown significantly increased N-cadherin, Vimentin, and Snail expression but decreased E-cadherin expression in GH3, MCF-7, and 293T cells. (C) Scratch assay of 293T and MCF7 cells with or without DLG1 siRNA; scale bar: 200 μm. Relative scratch

width over time shown below (n=3; mean ± SD shown below; P values by two-way ANOVA). (D) Transwell assay of 293T cells transfected with negative control (si-NC) and si-DLG1; scale bar: 200 μm. Data are presented as the mean ± SD from three independent experiments. P values by one-way ANOVA; **P<0.01; ***P<0.001; ****P<0.0001, relative to control (si-NC). (E) Confocal immunofluorescence images in wound healing migration assays of MCF7 cells. After transfection with siRNAs for 48 h, MCF7 cells were scratched to allow cell migration. Cells were fixed after migrating for 12 h, and then stained with phalloidin (green) and DAPI (blue) to reveal F actin and nuclei, respectively; scale bar: 50 μm.

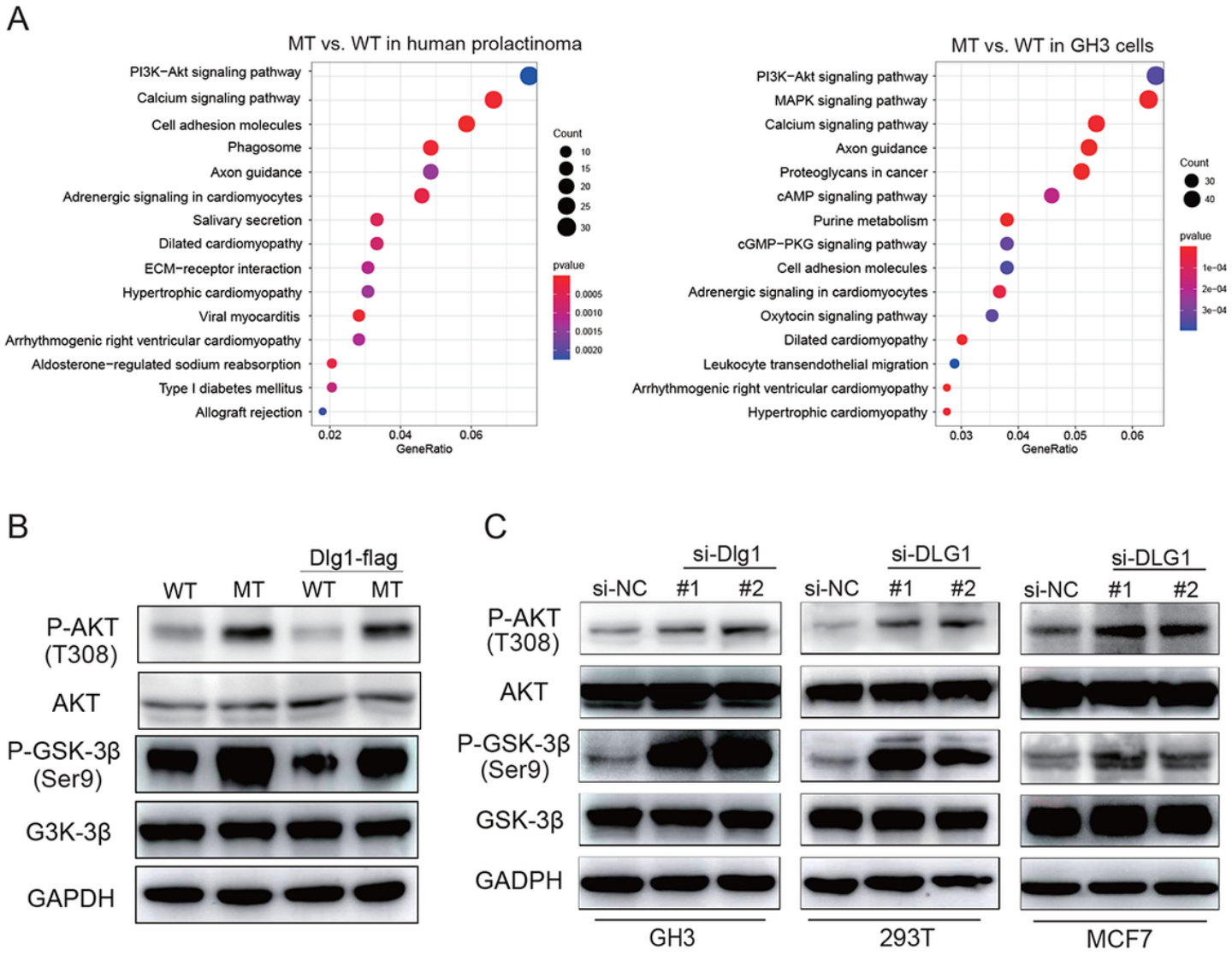

Figure 6

The SFB31/DLG1 axis promoted tumor invasion via the PI3K/AKT signaling pathway (A) KEGG enrichment analysis of DEGs in SF3B1 mutant vs. wild-type human prolactinoma and GH3 cells. (B) Phosphorylated and total AKT and GSK-3β levels in Sf3b1 WT and mutant GH3 cells transduced with or without Dlg1-FLAG cDNA. (C) Phosphorylated and total AKT and GSK-3β levels in GH3, 293T, and MCF7 cells transduced with or without DLG1 siRNA.

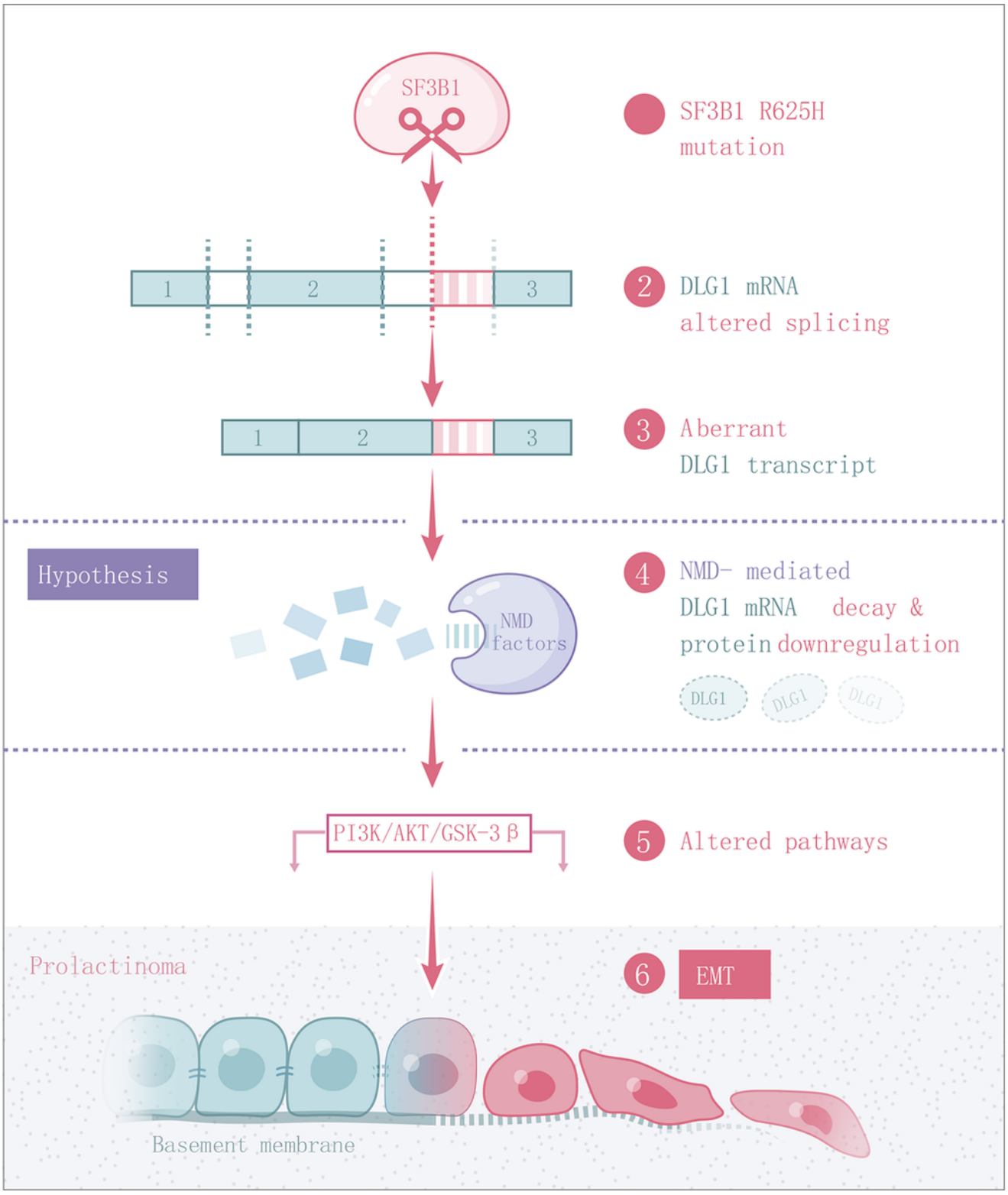

Figure 7

Schematic representation showing the proposed mechanisms through which the SF3B1 mutation promotes the prolactinoma progression.

Supplementary Files

This is a list of supplementary files associated with this preprint. Click to download.

- FigureS1.pdf
- FigureS2.pdf
- FigureS3.pdf
- FigureS4.pdf
- FigureS5.pdf
- SupplementalTables113.xlsx